A DFT study on carbon-doping at different sites of (8, 0) boron nitride nanotube. Struct Chem

ARTICLE *in* STRUCTURAL CHEMISTRY · APRIL 2012

Impact Factor: 1.84 · DOI: 10.1007/s11224-012-0110-3

2 AUTHORS:

Mehdi D Esrafili
University of Maragheh
179 PUBLICATIONS **899** CITATIONS
SEE PROFILE

Hadi Behzadi
28 PUBLICATIONS **204** CITATIONS
SEE PROFILE

Struct Chem
DOI 10.1007/s11224-012-0110-3

ORIGINAL RESEARCH

A DFT study on carbon-doping at different sites of (8, 0) boron nitride nanotube

Mehdi D. Esrafili · Hadi Behzadi

Received: 26 May 2012 / Accepted: 19 July 2012

Abstract A density functional theory study is carried out to investigate the geometries and electronic structure of pristine and carbon-doped (8, 0) single-walled boron nitride nanotubes (BNNTs). In order to understand the effect of impurities or doping on (8, 0) single-walled BNNT, we simulated C-doping in six different ways. Geometry optimizations reveal that in the considered models, B–N bond lengths are not significantly influenced by C-doping. Based on the quantum theory of atoms in molecules analysis, charge density accumulation for axial B–N bond critical points (BCPs) of pristine BNNT is slightly larger than zigzag ones. However, due to C-doping at the B- or N-tips, the evaluated electron density tends to decrease slightly at both axial and zigzag B–N BCPs. Besides, results indicate that influence of C-doping on properties of the (8, 0) BNNT could be also detected by values of chemical shielding isotropy (σ_{iso}) and anisotropy ($\Delta\sigma$).

Keywords (8, 0) BNNT · QTAIM · Bond critical point · NMR · Chemical shielding

Electronic supplementary material The online version of this article (doi:10.1007/s11224-012-0110-3) contains supplementary material, which is available to authorized users.

M. D. Esrafili (✉)
Laboratory of Theoretical Chemistry, Department of Chemistry, University of Maragheh, 5513864596, Maragheh, Iran
e-mail: esrafili@maragheh.ac.ir

H. Behzadi
Department of Chemistry, Kharazmi University, Mofatteh Avenue, Tehran, Iran

Introduction

Recently, much attention has been driven to boron nitride nanotubes (BNNTs) due to their unique and important properties, ideal for structural and electronic applications [1–8]. The BNNTs were successfully synthesized in 1995, shortly after their theoretical prediction, and a new area of nanotube science was born [9, 10]. The BNNTs are very similar to carbon nanotubes (CNTs) and they are basically regarded as isomorphic analogs of the CNTs. Their main difference is their conductivity. BNNTs are known as permanent semiconductors, with a constant band gap ($\approx$5.5 eV) nearly independent of tubular diameter and chirality [11, 12], while CNTs can show metallic or semiconductor behavior [13, 14]. Moreover, BNNTs present partially ionic B–N bonds which form a slight buckling on the tube surface. These two properties can be very important in building BNNTs covalently functionalized for nanoscale applications. Therefore, instead of CNTs, the BNNTs are expected to be more appropriate candidates for electronic and mechanical devices of specific purposes [15].

Many studies have demonstrated that electronic and structural properties of BNNTs can be significantly influenced by dopant atom [16, 17]. Up to now, doping BNNTs with different types of atoms is believed to be an effective way to enhance hydrogen storage capacity at ambient temperature [18–21]. In addition to increasing adsorption energy of H_2, metal doping also increases the effective surface area available for adsorption in some cases. Hydrogen adsorption then goes beyond a single monolayer, increasing the volumetric and gravimetric hydrogen densities accordingly [22]. In 2002, Pokropivnyi [23] suggested that "the BNNTs could be transformed into *n*- or *p*-type semiconductors by ionic doping." This might enable property control to meet different application requirements.

Published online: 18 August 2012

Although doped BNNTs have been realized experimentally [24, 25], it is very hard to verify the ordering and distribution of dopant atoms over atomic sites of a BNNT. A few ordering configurations were used in density functional theory-based calculations to estimate band gaps [26], magnetic properties [27, 28], and quadrupole coupling constants [29] of doped BNNTs. Determining the dependency of electronic structure on this ordering would help interpreting experimental observations. In fact, it is fundamentally crucial to understand how to modify the electronic structure of BNNTs through suitable doping. Here, we determine geometries and electronic structures of zigzag (8, 0) BNNT with various distributions of dopant atoms. The influence of C-doping on different sites of a zigzag (8, 0) BNNT model is examined based on structural parameters such as optimized bond lengths and dipole moments. From the set of theories with the capability of describing local variations of bonding, the quantum theory of atoms in molecules (QTAIM) approach [30] was also selected for the current study. In addition, chemical shielding tensors at ^{11}B and ^{15}N nuclei are calculated for the different C-doped BNNTs. Section "Computational aspects" illustrate the details of quantum chemistry calculations used in this work, and the effect of C-doping on structural parameters and electronic structures of zigzag (8, 0) BNNT is discussed in the "Results and discussion" section. We particularly focus our discussions on the electronic charge redistribution due to the carbon-doping, and sum up in the "Concluding remarks" section. This research aims to clarify the effect of C-doping on the electronic structure and properties of BNNTs and give insight about the nature of B–N, C–B, and C–N in these systems. The consistency of Bader theory results with DFT bond lengths and chemical shielding tensors would also be discussed.

Computational aspects

All molecular orbital calculations are performed by means of the Gaussian 03 suite of programs [31]. The geometry of the investigated pristine and C-doped BNNTs is optimized at the B3LYP level [32, 33] by means of 6-31G* basis set. It is noteworthy to mention that the size of the model and the level of theory employed for studying the electronic structure of nanotubes are validated by the results acquired from our previous work [34].

QTAIM methodology (AIM2000 program [35] at B3LYP/6-31G* computational level) is applied to analyze electron density of the systems [30]. For atom–atom interactions such as intermolecular contacts or valence bonds, the characteristics of the corresponding bond critical point (BCP) of molecular charge density, ρ_{BCP}, are very important. These are points where the electron density gradient $\nabla\rho_{\mathrm{BCP}}$ vanishes and additional characterization is done by the corresponding Hessian matrix (a 3 × 3 matrix of second derivatives). Diagonalization of this matrix yields the coordinate invariant eigenvalues: $\lambda_1 \leq \lambda_2 \leq \lambda_3$. Laplacian, $\nabla^2\rho_{BCP}$, of charge density at the bond critical point is defined as:

$$\nabla^2\rho_{\mathrm{BCP}} = \sum_{i=1}^{3}\lambda_i \tag{1}$$

and the relation between energetic topological parameters and Laplacian of electron density at BCP is known to be:

$$\frac{1}{4}\nabla^2\rho_{\mathrm{BCP}} = 2G_{\mathrm{BCP}} + V_{\mathrm{BCP}} \tag{2}$$

$$H_{\mathrm{BCP}} = G_{\mathrm{BCP}} + V_{\mathrm{BCP}} \tag{3}$$

where G_{BCP}, V_{BCP}, and H_{BCP} are the kinetic, potential, and total electronic energy densities at critical point, respectively. G_{BCP} is a positive value, whereas V_{BCP} is a negative one. Ellipticity, ε, is defined as:

$$\varepsilon = (\lambda_1/\lambda_2) - 1 \tag{4}$$

Bond ellipticity is a measure of stability, and higher values indicate instability of the corresponding bond [36].

Chemical shielding tensors are calculated for the optimized structures at B3LYP/6-31G* level of theory by means of the gauge included atomic orbital method (GIAO) [37]. Quantum chemical calculations yield chemical shielding tensors in the principal axis system (PAS) with the order of $\sigma_{33} > \sigma_{22} > \sigma_{11}$; hence, Eqs. (4) and (5) are used to convert the calculated chemical shielding tensors to the absolute isotropic (σ_{iso}) and anisotropic ($\Delta\sigma$) chemical shielding parameters:

$$\sigma_{\mathrm{iso}} = (\sigma_{11} + \sigma_{22} + \sigma_{33})/3 \tag{5}$$

$$\Delta\sigma = \sigma_{33} - (\sigma_{11} + \sigma_{22})/2 \tag{6}$$

Results and discussion

Structural parameters and band gaps

The optimized pristine and C-doped (8, 0) BNNTs are shown in Fig. 1. The pristine model (Fig. 1a) stands for the original structure of BNNT, consisting of B and N atoms. In order to understand the effect of impurities or doping on (8, 0) single-walled BNNT, C-doping is simulated in six different ways: (a) a single C layer doped at the B-tip (C_{B4}), (b) a single C layer doped at the N-tip (C_{N1}), (c) two C layers co-doped at both B- and N-tips ($C_{B4\text{-}N1}$), (d) a single C layer doped at the internal B sites (C_{B2}), (e) a single C layer doped at the internal N sites (C_{N3}), and (f) C-doped at B and N sites along the tube axis ($C_{BN\text{-}axis}$).

All these C-doping possibilities are examined for (8, 0) zigzag BNNT in isolated form for all models of the investigated (8, 0) BNNT.

Table 1 summarizes the equilibrium bond lengths, dipole moments, and band gaps for all the models at equilibrium bond lengths. There are two nonequivalent B–N bonds in pristine (8, 0) BNNT: axial B–N bonds, parallel to the longitudinal direction of tube (e.g., the bond between B1 and N2 layers in Fig. 1a), and zigzag B–N bonds (e.g., the bond between B1 and N1 layers in Fig. 1a). In general, the B–N bond lengths are not significantly changed upon C-doping in the considered models (Table 1). However, different B–C and C–N bond distances are evident where the latter is slightly shorter than the former. For example, the C–B bond length in the $C_{B4–N1}$ model is calculated to be 1.520 Å, whereas C–N bond length is about 1.433 Å. Although our estimates of C–B and B–N contacts in doped (8, 0) BNNTs agree well with earlier works (within 0.5 %) [26], the evaluated bond C–N length deviates by up to 4–5 %. This is understandable in terms of the difference in exchange–correlation functionals used here [26]. It is worth mentioning that the N-tip diameter is larger than the B-tip in the pristine model. The case is also evidenced for C-doped models, while widening of the B-tip due to the doping procedure is more significant than the N-tip. Interestingly, C-doping at one tip in C_{B4} or C_{N1} does not change the tip diameter compared to the $C_{B4–N1}$ model. This means that in the investigated models of the (8, 0) BNNT, an individual tips do not detect changes in the other tip, and this validates the size of models used in this study.

It is expected that the C-doping at the B-tip of (8, 0) BNNT is associated with a dipole moment enhancement due to charge transfer and electron delocalization of C atoms. Dipole moments (μ) of the (8, 0) BNNTs are listed in Table 1. In zigzag (8, 0) BNNT, unlike nonpolar cases of hexa-boron nitride (hBN) and armchair BNNTs, the dipole moment is nonzero due to alternate layers of B and N atoms [38]. As electronegativity of the N atom is larger

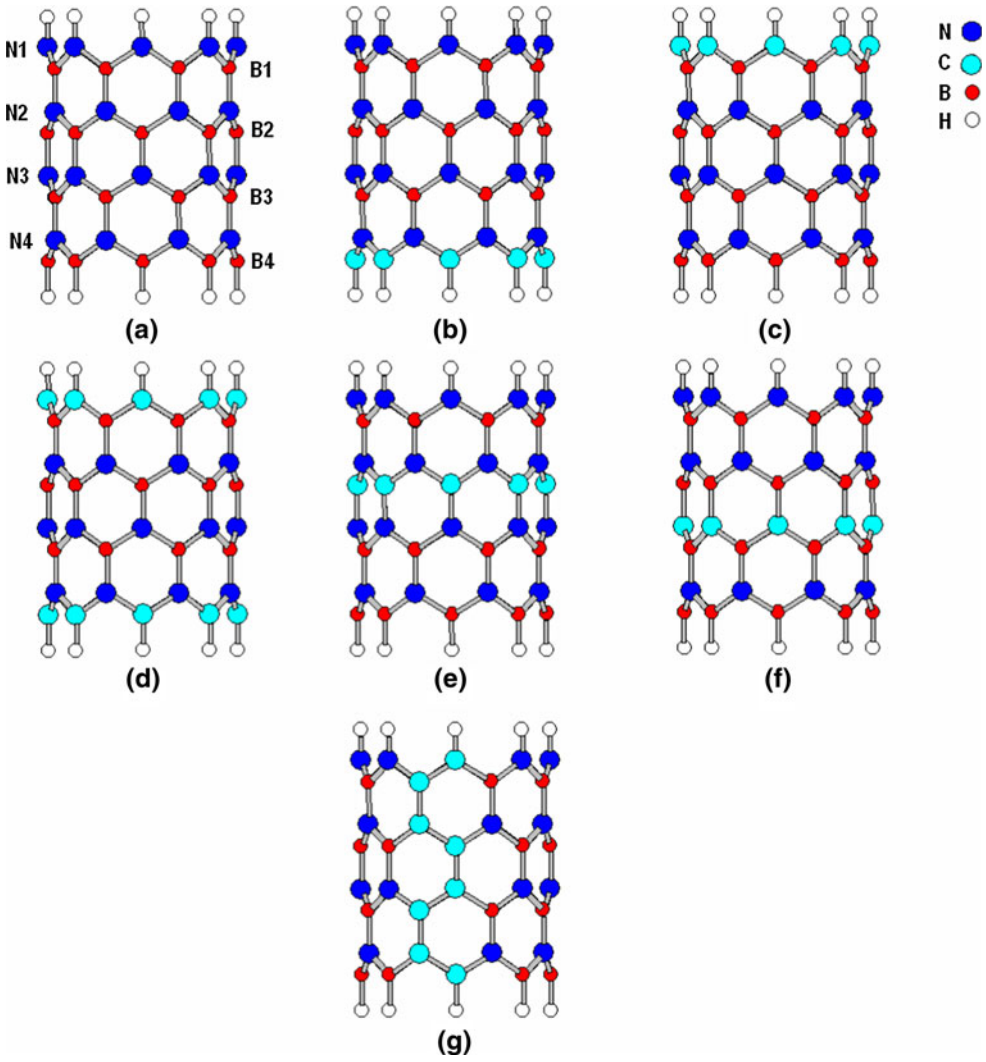

Fig. 1 The molecular models of investigated (8, 0) BNNT: **a** the pristine model, **b** the C-doping at the B-tip (C_{B4} model), **c** the C-doping at the N-tip (C_{N1} model), **d** the two C layers co-doped at both B- and N-tips ($C_{B4\text{-}N1}$ model), **e** a single C layer doped at the inner B sites (C_{B2} model), **f** a single C layer doped at inner N sites (C_{N3} model), and **g** C-doping along the tube axis ($C_{BN\text{-}axis}$)

Table 1 Calculated bond distances (in Å), dipole moment (in Debye), and band gap (in eV) of pristine and C-doped (8, 0) BNNTs

Bond	Bond length						
	Pristine	C_{B4}	C_{N1}	$C_{B4–N1}$	C_{B2}	C_{N3}	$C^{a}_{BN\text{-}axis}$
$r_{N1–B1}$	1.448	1.447	–	–	1.435	1.447	1.447
$r_{B1–N2}$	1.452	1.454	1.461	1.498	1.456	1.454	1.454
$r_{N2–B2}$	1.453	1.456	1.461	1.443	–	1.466	1.452
$r_{B2–N3}$	1.450	1.451	1.448	1.491	–	–	1.452
$r_{N3–B3}$	1.452	1.452	1.454	1.431	1.473	–	1.451
$r_{B3–N4}$	1.454	1.459	1.453	1.492	1.450	1.461	1.455
$r_{N4–B4}$	1.451	–	1.451	–	1.448	1.458	1.450
$r_{N4–C}$	–	1.491	–	1.433	–	–	–
$r_{B1–C}$	–	–	1.542	1.520	–	–	–
$r_{N2–C}$	–	–	–	–	1.350	–	–
$r_{C–N3}$	–	–	–	–	1.373	–	–
$r_{B2–C}$	–	–	–	–	–	1.561	–
$r_{B3–C}$	–	–	–	–	–	1.513	–
μ (Debye)	11.26	12.21	6.24	17.25	13.50	14.53	7.29
Band gap (eV)	5.63	1.63	0.49	0.60	1.88	0.49	3.65

[a] Mean B–N values

than B and C, C-doping of N-tips exerts the minimal value of the dipole moment compared to the other models, and C-doping is found to reduce the value of the dipole moment in case of the C_{N1}-doped model. A relatively higher value of the dipole moment is evidenced for the $C_{B4–N1}$-doped model due the fact that this nanotube has C-doped layers on either B or N-tips and thus the two ends of nanotube will always be populated by the same kinds of atoms. Comparing the dipole moments in C_{B2} and C_{N3} models, it becomes evident that substitution of C atoms at the inner B and N sites increases the μ value by 2.3 and 3.4 Debye, respectively. Besides, C-doping reduces the value of the dipole moment in the case of $C_{BN\text{-}axis}$, which can be attributed to the decreased charge difference between the layers (Table 1).

The highest occupied molecular orbital (HOMO) and the lowest unoccupied molecular orbital (LUMO) of different (8, 0) BNNT models are presented in form of isosurface plots (Fig. 2). In pristine (8, 0) BNNT, the HOMO corresponds to isolated electron pairs localized at N atoms and has the spindle-shaped scheme like p_z orbitals, whereas LUMO presents π states localized at B–N pair along the tube axis and is contributed by the N-2*p* (major) and B-2*p* (minor) states. From Fig. 2, it is evident that for C-doping at B- or N-tips, the major contribution to electron density comes from dopant atoms. HOMO for models doped at the B-tip has the major part from carbon *p*-states and a partial contribution from nitrogen *p*-states (see Fig. 2), meaning that the state is relatively localized. However, parts of the charge on the highest-energy occupied 2*p* orbitals of B atoms around move to the C atom, and its HOMO mainly consists of isolated electron pairs at C atoms (Fig. 2e). Alternatively, for a single C layer doping at the N-tip (C_{N1} model), both the HOMO and LUMO show remarkable contribution from dopant states, the LUMO is a localized state with mainly nitrogen *p* character. For a BNNT with B–N pair doping ($C_{BN\text{-}axis}$), both HOMO and LUMO have a major contribution from carbon *p*-states. Besides, the gap between HOMO and LUMO for pristine (8, 0) BNNT is calculated to be 5.63 eV, consistent with the experimentally measured value: 5.8 (±0.2 eV) [39]. The results also indicate that band gap of the C-doped models is smaller than that of the pristine one and among the C-doped models, the most significant changes are found for C_{N1} and C_{N3}-doped models (i.e., C-doping at the N-tip and inner N layer, respectively). The decreased band gap enhances the reactivity of C-doped BNNT, particularly at C sites, making it more conductive.

QTAIM analysis

It is well known that substitution of carbon atoms at the B or N sites is followed by some electron density redistribution in BNNT. Detailed information about the nature and strength of B–N, C–N, and B–C contacts can be obtained from topological analysis of electron density. Application of QTAIM for all the above discussed (8, 0) BNNT models allows finding BCPs and analyzing their properties. Based on QTAIM, the large ρ_{BCP} values and values of $\nabla^2\rho_{BCP} < 0$ refer to the covalent bond, while small ρ_{BCP} values and values of $\nabla^2\rho_{BCP} > 0$ are calculated for closed-shell and ionic interactions [36]. According to QTAIM, the bonded atoms are characterized by duo-gradient paths of

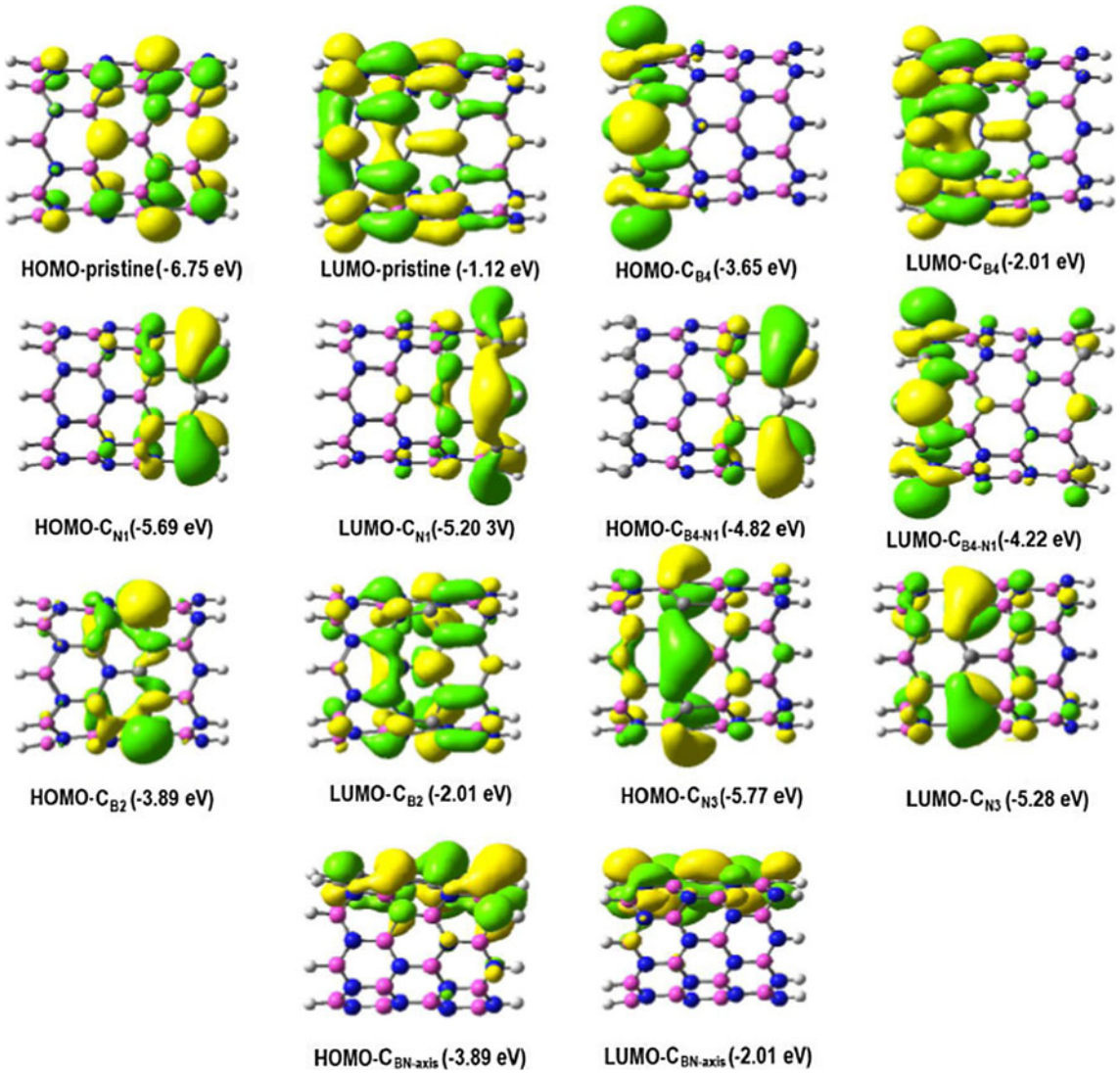

Fig. 2 Isosurfaces of HOMO and LUMO for pristine and C-doped (8, 0) BNNTs (isovalue = 0.02 e/bohr3)

the charge density function, which originate from a BCP and terminate on corresponding atomic nuclei. These gradient paths which are at equilibrium geometry, called ''bond paths,'' must be regarded as ''universal indicators of bonded interactions.'' The quantum mechanical structure is proposed by molecular graph which is a collection of BCPs and their associated bond paths.

Figure 3 exhibits molecular graph of pristine (8, 0) BNNT in its equilibrium geometry. ρ_{BCP} and $\nabla^2\rho_{BCP}$ at BCP of B–N, B–C, and N–C bond paths of (8, 0) BNNTs are given in Table 2. One of the most striking features of these results is the fact that all calculated ρ_{BCP} values in B–N of pristine (8, 0) BNNT are in the range of 0.190–0.194 au, while $\nabla^2\rho_{BCP}$ values are all positive, ranging from 0.288 to 0.337 au. These values are within the common accepted values for closed-shell interactions [36]. It should be noted that the ρ_{BCP} value at the BCP of B–N bonds of BNNT is considerably smaller than that obtained for C–C bonds of CNTs [40]. More specifically, QTAIM analysis indicates that charge density accumulation for axial B–N bonds is slightly larger than the zigzag ones. $\nabla^2\rho_{BCP}$ evaluated for axial bonds, on the other hand, is slightly smaller than that of the zigzag ones. Our calculations reveal that due to C-doping at B- or N-tips, the evaluated electron density tends to decrease slightly at both axial and zigzag B–N BCPs. As evident from Table 2, the diminution of charge density is more significant for neighbor axial B–N bonds. The corresponding Laplacian of electron density, however, increases upon C-doping at the two tips. It is also found that the evaluated ρ_{BCP} at N4–C critical points of the C_{B4}-doped model is larger than that of B1–C in the C_{N1} model. The $\nabla^2\rho_{BCP}$ values estimated for N4–C and B1–C in C_{B4} and C_{N1} models are −0.970 au and −0.066 au, respectively, indicative of a covalent nature of

these bonds. In case of C_{B2}, axial B1–N2, B2–N3, and N4–B3 bonds in C-doped BNNT lose electrons at their BCPs, while the zigzag bonds gain electrons. Notably, ρ_{BCP} at the N–C BCPs is slightly larger than B–C bonds, confirming the strength of the former one. However, a more significant change is found in ρ_{BCP} and $\nabla^2\rho_{BCP}$ parameters of C_{B2} and C_{N3} models where C atoms are doped at B2 and N3 layers, respectively. The mean charge density at the B–N BCPs of the $C_{BN\text{-}axis}$-doped model is not significantly changed upon C-doping along the tube axis (Table 1). Nevertheless, different ρ_{BCP} values of B–C and C–N BCPs are also evident, with the latter slightly larger.

According to Rozas et al. [41], the character of interaction could be classified as a function of H_{BCP} with Laplacian of electron density at BCP. This means that for strong interactions ($\nabla^2\rho_{BCP} < 0$ and $H_{BCP} < 0$), the covalent character is established; for medium strength ($\nabla^2\rho_{BCP} > 0$ and $H_{BCP} < 0$), their partially covalent character is defined; and weak ones ($\nabla^2\rho_{BCP} > 0$ and $H_{BCP} > 0$) are mainly electrostatic. Thus, magnitude of H_{BCP} reflects the "degree of covalency" in a given interaction. Based on the evaluated H_{BCP} values for the studied BNNT models (Table S1; Supporting Information), all B–N interactions in pristine (8, 0) BNNT have a negative H_{BCP} value, showing a partially covalent character. However, a covalent interaction is evident in the B–C and N–C-doped bonds. Our calculations reveal that C-doping at the B-tip gives the most covalent N–C bond, whereas B–C bonds in the C-doped at the N-tip have the smallest covalency.

As shown earlier [36], bond ellipticity, ε, is a measure of π-character of bonding up to the limit of ''double bond'' for which the ellipticity reaches a maximum. For pristine (8, 0) BNNT, the calculated ε values are in the range of 0.042–0.141 where the highest π-character belongs to N4–B4 bonds. As in Table S1, C-doping at different sites of BNNT has a significant influence on ε. In case of C_{B4}-doped models, for instance, doping decreases the evaluated ε in zigzag bonds, whereas a reverse trend is found for axial bonds. ε for B–C bonds in the C_{N1}-model is 0.103, exhibiting some potential π-character. Moreover, the ellipticity along the C–B bond path indicates a very asymmetric contribution to the π-bond from the two atoms.

NMR parameters

In this section, we discuss the evaluated NMR parameters at ^{11}B and ^{15}N sites for different BNNTs. NMR spectra yield a wealth of information with the most commonly reported property being the chemical shielding tensor [38]. This parameter relates an externally applied magnetic field to the changes in the local electronic environment of the magnetic nuclei. Hence, a key insight into the underlying atomic structure is provided. The NMR parameters are strongly dependent on molecular structure and structural parameters that exist within a molecule. Besides, performing an experimental NMR study on BNNTs is a formidable task due to the complexity of the electronic environment of BNNTs. To the best of our knowledge, there exist no experimental NMR reports on BNNTs. Therefore, to verify the reliability of the NMR parameters evaluated in this study, we would trust the employed computational level for reproduction of NMR parameters in BNNTs [42].

Table 3 gives the calculated chemical shielding isotropy (σ_{iso}) and anisotropy ($\Delta\sigma$) parameters at the sites of ^{11}B and ^{15}N nuclei of seven optimized models of the zigzag (8, 0) BNNT (Fig. 1). The evaluated NMR parameters are divided into four layers for the models, according to the similarities in parameters for each layer. In pristine BNNT, the

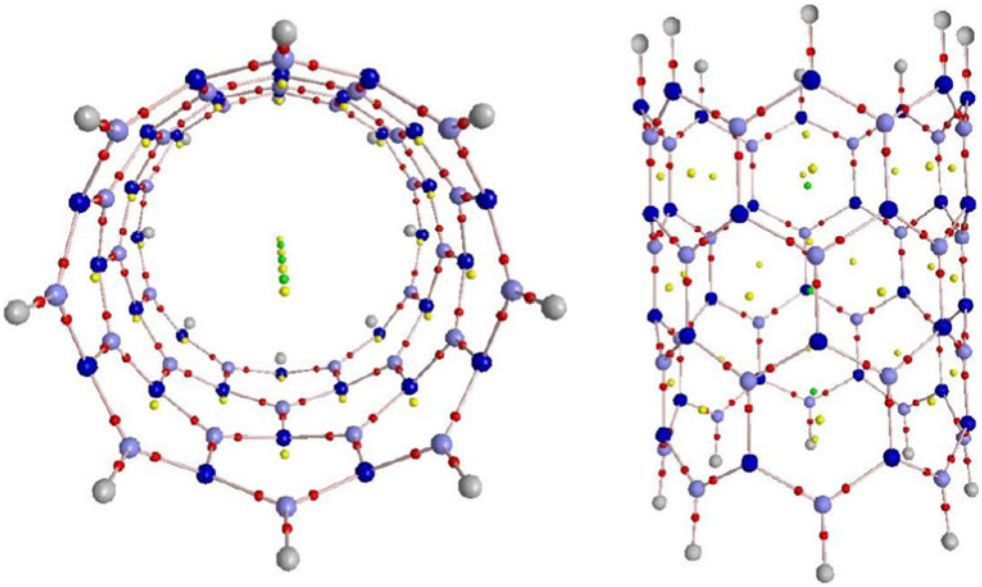

Fig. 3 *Top* and *side* views of the molecular graph of pristine (8, 0) BNNT. The graph was obtained at the B3LYP/6-31G* level. *Big circles* correspond to attractors and *small red* and *yellow circles* are bond and ring critical points, respectively. The *lines* are bond paths (Color figure online)

Table 2 The calculated QTAIM parameters (in au) of pristine and C-doped (8, 0) BNNTs

Bond	Pristine		C_{B4}		C_{N1}		$C_{B4–N1}$		C_{B2}		C_{N2}		$C^{a}_{BN\text{-}axis}$	
	ρ_{BCP}	$\nabla^2\rho_{BCP}$	ρ_{BCP}	$\nabla^2\rho_{BCP}$	ρ_{BCP}	$\nabla^2\rho_{BCP}$	ρ_{BCP}	$\nabla^2\rho_{BCP}$	ρ_{BCP}	$\nabla^2\rho_{BCP}$	ρ_{BCP}	$\nabla^2\rho_{BCP}$	ρ_{BCP}	$\nabla^2\rho_{BCP}$
N1–B1	0.191	0.336	0.191	0.338	–	–	–	–	0.196	0.368	0.192	0.338	0.191	0.337
B1–N2	0.194	0.296	0.193	0.295	0.184	0.385	0.166	0.367	0.189	0.359	0.194	0.282	0.193	0.296
N2–B2	0.192	0.309	0.193	0.311	0.192	0.309	0.199	0.308	–	–	0.188	0.317	0.192	0.309
B2–N3	0.194	0.312	0.191	0.313	0.193	0.317	0.173	0.316	–	–	–	–	0.193	0.311
N3–B3	0.192	0.312	0.193	0.346	0.193	0.316	0.203	0.321	0.202	0.413	–	–	0.192	0.313
B3–N4	0.194	0.288	0.190	0.348	0.194	0.289	0.172	0.363	0.196	0.286	0.185	0.368	0.193	0.287
N4–B4	0.190	0.337	–	–	0.190	0.337	–	–	0.191	0.349	0.188	0.323	0.190	0.338
N4–C	–	–	0.335	−0.970	–	–	0.263	−0.577	–	–	–	–	–	–
B1–C	–	–	–	–	0.182	−0.066	0.192	−0.111	–	–	–	–	–	–
N2–C	–	–	–	–	–	–	–	–	0.207	−0.394	–	–	–	–
N3–C	–	–	–	–	–	–	–	–	0.262	−0.704	–	–	–	–
B2–C	–	–	–	–	–	–	–	–	–	–	0.181	−0.244	–	–
B3–C	–	–	–	–	–	–	–	–	–	–	0.185	−0.093	–	–

[a] Mean ρ_{BCP} and $\nabla^2\rho_{BCP}$ values at B–N BCPs

largest value of σ_{iso} (^{11}B) and $\Delta\sigma$(^{11}B) belongs to the B1-layer which is the first neighbor of the N-tip. For the ^{15}N nuclei, the largest value of σ_{iso} and $\Delta\sigma$ parameters belongs to the N4-layer which is the first neighbor of the B-tip of the nanotubes. Such a different behavior of NMR parameters can be attributed to the natures of valence shells of the N atoms, having lone pair of electrons, and the B atoms, which lack electron. It is also noted that magnitudes of the changes in NMR parameters of ^{15}N atoms are larger than ^{11}B atoms. Furthermore, the larger values of σ_{iso} in N1- and B1-layers reveal that chemical bonding of B1–N1 could be different from B4–N4. In C_{B4}- and C_{N1}-doped models, the atoms in B4 and N1-layers are substituted by C atoms. Similarities in NMR parameters for the atoms of each layer are also observed for these models. NMR calculations reveal that σ_{iso} and $\Delta\sigma$ values of N1- and B1-layers are not influenced by C-doping in the B-tip, but the other layers detect changes. σ_{iso} and $\Delta\sigma$ parameters calculated for the atoms in the N4-layer, which are in direct chemical bonding with C atoms, decrease. The value of σ_{iso}(^{11}B) for the B1-layer in the C_{N1}-doped model is smaller than the pristine model, showing that the atoms in this layer produce stronger chemical bonding with the doped C atoms. The value of σ_{iso} in the N4-layer does not change, which means that the strength of bonding for the N atoms in the N4-layer is shared with the C atoms from the C-terminated layer. In the C_{B2}-doped model, the chemical shielding tensors at B1 and B3 sites also undergo significant changes due to chemical bonding to the carbon atoms; therefore, the value of σ_{iso}(^{11}B) for these nuclei slightly increases compared to the pristine model. Considering the carbon atoms' substitution at the N3 layer, the chemical shielding tensors at the sites of N2 and N4 also undergo notable changes due to C-doping, whereas the changes at N1 are almost negligible. This trend reveals that the chemical shielding tensors at the N sites directly bonded to C atom undergo significant changes, while the other N nuclei do not sense variations. Comparing the NMR parameters reveals that the electronic

Table 3 Calculated NMR parameters (in ppm) of pristine and C-doped (8, 0) BNNTs

Nuclei	Pristine		C_{B4}		C_{N1}		$C_{B4–N1}$		C_{B2}		C_{N2}		$C^{a}_{BN\text{-}axis}$	
	σ_{iso}	$\Delta\sigma$	σ_{iso}	$\Delta\sigma$	σ_{iso}	$\Delta\sigma$	σ_{iso}	$\Delta\sigma$	σ_{iso}	$\Delta\sigma$	σ_{iso}	$\Delta\sigma$	σ_{iso}	$\Delta\sigma$
^{11}B1	73	41	73	41	52	99	67	74	76	40	83	32	73	41
^{11}B2	71	38	71	37	64	53	76	33	–	–	89	48	72	38
^{11}B3	72	40	73	36	71	35	78	33	79	31	27	132	72	40
^{11}B4	67	55	–	–	69	50	–	–	68	54	72	57	66	55
^{15}N1	156	75	156	77	–	–	–	–	157	99	194	56	157	74
^{15}N2	125	188	124	188	231	314	93	249	73	195	241	301	126	189
^{15}N3	122	197	120	224	135	170	104	247	121	170	–	–	122	197
^{15}N4	87	244	45	222	93	233	13	274	87	242	113	214	87	246

[a] Mean σ_{iso} and $\Delta\sigma$ values were used for each layer

structure of the $C_{BN\text{-}axis}$ model, where the B–N bonds along the tube axis are doped by the C atoms, is less influenced than the other models. This finding is better proven by the differences between B–N bond lengths and QTAIM parameters of the different C-doped BNNT models.

Concluding remarks

In this paper, the electronic structure properties of pristine and C-doped (8, 0) BNNTs were investigated by performing DFT calculations. In order to understand the effect of impurities or doping on (8, 0) single-walled BNNT, C-doping was investigated in six different ways including (a) a single C layer doped at the B-tip (C_{B4}), (b) a single C layer doped at the N-tip (C_{N1}), (c) two C layers co-doped at both B- and N-tips ($C_{B4\text{-}N1}$), (d) a single C layer doped at the inner B sites (C_{B2}), (e) a single C layer doped at the inner N sites (C_{N3}), and (f) C-doped at B and N sites along the tube axis ($C_{BN\text{-}axis}$).

1) B3LYP/6-31G* calculations indicated that B–N bond lengths are not changed as a result of C-doping. However, C–N bond distance is slightly shorter than B–C.
2) In the C-terminated models, tubular diameter of the B-tip in BNNT is wider than the N-tip.
3) C-doping reduces the value of the dipole moment in case of the C_{N1}-doped model. Since electronegativity of N atom is larger than B and C, C-doping of the N-tip exerts the most significant influence on the value of the dipole moment.
4) Based on QTAIM results, it can be concluded that all B–N interactions in the pristine (8, 0) BNNT have a negative H_{BCP} value and thus have partially covalent character. However, covalent interaction is evident for the B–C and N–C-doped bonds. Moreover, ρ_{BCP} at N–C BCPs is slightly larger than those of B–C bonds, which confirms that the former is stronger than the latter.
5) The evaluated NMR parameters are divided into four layers for the models, regarding similarities in the parameters for each layer. In pristine BNNT, the largest value of σ_{iso} (^{11}B) and $\Delta\sigma$ (^{11}B) belongs to the B1-layer which is the first neighbor of the N-tip. For the ^{15}N nuclei, the largest σ_{iso} and $\Delta\sigma$ value is attributed to the N4-layer which is the first neighbor of the B-tip in nanotubes.

References

1. Zhi C, Bando Y, Tang C, Golberg D (2010) Boron nitride nanotubes. Mater Sci Eng 70:92–111
2. Akdim B, Pachter R, Duan X, Adams WW (2003) Comparative theoretical study of single-wall carbon and boron-nitride nanotubes. Phys Rev B 67:245404
3. Won CY, Aluru NR (2008) Water phase transition induced by a Stone–Wales defect in a boron nitride nanotube. J Am Chem Soc 130:13649–13652
4. Han WQ, Zettl A (2003) Functionalized boron nitride nanotubes with a stannic oxide coating: a novel chemical route to full coverage. J Am Chem Soc 125:2062–2063
5. Xie SY, Wang W, Fernando KAS, Wang X, Lin Y, Sun YP (2005) Solubilization of boron nitride nanotubes. Chem Commun 29:3670–3672
6. Mpourmpakis G, Froudakis GE (2007) Why boron nitride nanotubes are preferable to carbon nanotubes for hydrogen storage?: an ab initio theoretical study. Catal Today 120:341–345
7. Schmidt TM, Baierle RJ, Piquini P, Fazzio A (2003) Theoretical study of native defects in BN nanotubes. Phys Rev B 67:113407
8. Beheshtian J, Behzadi H, Esrafili MD, Shirvani BB, Hadipour NL (2011) A computational study of water adsorption on boron nitride nanotube. Struct Chem 21:903–908
9. Chropra NG, Luyken RJ, Cherrey K, Crespi VH, Cohen ML, Louie SG, Zettl A (1995) Boron nitride nanotubes. Science 269:966–967
10. Goldberg D, Bando Y, Han W, Kurashima K, Sato T (1999) Single-walled B-doped carbon, B/N-doped carbon and BN nanotubes synthesized from single-walled carbon nanotubes through a substitution reaction. Chem Phys Lett 308:337–342
11. Rubio A, Corkill JL, Cohen ML (1994) Theory of graphitic boron nitride nanotubes. Phys Rev B 49:5081–5084
12. Blase X, Rubio A, Louie SG, Cohen ML (1994) Stability and band gap constancy of boron nitride nanotubes. Europhys Lett 28:335–340
13. Hamada N, Sawada S, Oshiyama A (1992) New one-dimensional conductors: graphitic microtubules. Phys Rev Lett 68:1579–1581
14. Saito R, Fujita M, Dresselhaus G, Dresselhaus MS (1992) Electronic structure of chiral graphene tubules. Appl Phys Lett 60:2204–2206
15. Radosavljevic M, Appenzeller J, Derycke V, Martel R, Avouris P, Loiseau A, Cochon JL, Pigache D (2003) Electrical properties and transport in boron nitride nanotubes. Appl Phys Lett 82: 4131–4133
16. Tang C, Bando Y, Huang Y, Yue S, Gu C, Xu F, Golberg D (2005) Fluorination and electrical conductivity of BN nanotubes. J Am Chem Soc 127:6552–6553
17. Wu RQ, Liu L, Peng GW, Feng YP (2005) Magnetism in BN nanotubes induced by carbon doping. Appl Phys Lett 86: 122510–122512
18. Baierle RJ, Piquini P, Schmidt TM, Fazzio A (2006) Hydrogen adsorption on carbon-doped boron nitride nanotube. J Phys Chem B 110:21184–21188
19. Jhi SH, Kwon YK (2004) Hydrogen adsorption on boron nitride nanotubes: a path to room-temperature hydrogen storage. Phys Rev B 69:245407–245410
20. Venkataramanan NS, Belosludov RV, Sahara R, Mizuseki H, Kawazoe Y (2010) Theoretical investigation on the alkali–metal doped BN fullerene as a material for hydrogen storage. Chem Phys 377:54–59
21. Durgun E, Jang YR, Ciraci S (2007) Hydrogen storage capacity of Tidoped boron–nitride and B/Be-substituted carbon nanotubes. Phys Rev B 76:073413–073414
22. Cho JH, Yang SJ, Lee K, Park CR (2011) Si-doping effect on the enhanced hydrogen storage of single walled carbon nanotubes and grapheme. Int J Hydrogen Energy 36:12286–12295
23. Pokropivnyi VV (2002) Powder Metallurgy Metal Ceram. 41:123–135

24. Liu J, Czrew R, Carroll DL (2005) Large-scale synthesis of highly aligned nitrogen doped carbon nanotubes by injection chemical vapor deposition methods. J Mater Res 20:538–543
25. Terrones M, Romo-Herrera JM, Cruz-Silva E, López-Urías F, Munoz-Sandoval E, Velázquez-Salazar JJ, Terrones H, Bando Y, Golberg D (2007) Mater Today 53:30–38
26. Zhao JX, Tian Y, Dai BO (2005) A theoretical study on the conductivity of carbon doped BNNT. J Chin Chem Soc 52:395–398
27. Kahaly MU, Waghmare UV (2008) Contrast in the electronic and magnetic properties of doped carbon and boron nitride nanotubes: a first-principles study. J Phys Chem C 112:3464–3472
28. Mirzaei M, Nouri A (2010) The Al-doped BN nanotubes: a DFT study. J Mol Struct: THEOCHEM 942:83–87
29. Mirzaei M, Hadipour NL, Abolhassani MA (2007) Influence of C-doping on the B-11 and N-14 quadrupole coupling constants in boron-nitride nanotubes: a DFT study. Z Naturforsch 62a:56–60
30. Bader RFW (1990) Atoms in molecules-a quantum theory. Oxford University Press, New York
31. Frisch MJ, Trucks GW, Schlegel HB, Scuseria GE, Robb MA, Cheeseman JR, Zakrzewski VG, Montgomery JA, Stratmann RE, Burant JC, Dapprich S, Millam JM, Daniels AD, Kudin KN, Strain MC, Farkas O, Tomasi J, Barone V, Cossi M, Cammi R, Mennucci B, Pomelli C, Adamo C Clifford S, Ochterski J, Petersson GA, Ayala PY, Cui Q, Morokuma K, Malick DK, Rabuck AD, Raghavachari K, Foresman JB, Cioslowski J, Ortiz JV, Stefanov BB, Liu G, Liashenko A, Piskorz P, Komaromi I, Gomperts R, Martin RL, Fox DJ, Keith T, Al-Laham MA, Peng CY, Nanayakkara A, Gonzalez C, Challacombe M, Gill PMW, Johnson B, Chen W, Wong MW, Andres JL, Head-Gordon M, Replogle ES, Pople JA (2003) Gaussian Inc., Pittsburgh PA
32. Becke AD (1988) Density-functional exchange–energy approximation with correct asymptotic behavior. Phys Rev A 38:3098–3100
33. Lee C, Yang W, Parr RG (1988) Development of the Colle–Salvetti correlation-energy formula into a functional of the electron density. Phys Rev B 37:785–789
34. Zhao J, Ding Y (2009) The effects of O_2 and H_2O adsorbates on field-emission properties of an (8, 0) boron nitride nanotube: a density functional theory study. Nanotechnology 20:085704–085709
35. Biegler-Konig F, Schonbohm J, Bayles D (2001) AIM 2000. J Comput Chem 22:545–559
36. Popelier P (2000) Atoms in molecules, an introduction. Prentice-Hall, Englewood Cliffs, NJ
37. Duer MJ (2002) Solid state NMR spectroscopy. Blackwell Science Ltd., London, p 2002
38. Erkoç S (2003) Structural and electronic properties of single-wall BN nanotubes. J Mol Struct: THEOCHEM 542(2003):89–93
39. Arenal R, Stéphan O, Kociak MD, Taverna AL, Colliex C (2005) Electron energy loss spectroscopy measurement of the optical gaps on individual boron nitride single-walled and multiwalled nanotubes. Phys Rev Lett 95:127601–127604
40. Rashidi-Ranjbar P, Sadjadi A, Shafiee GH, Foroutan-Nejad C (2008) Application of quantum theory of atoms in molecules on small single wall (6, 0) zigzag carbon clusters. Part I: topological analysis of electron density, structure and bonding. J Mol Struct: THEOCHEM 856:79–87
41. Rozas I, Alkorta I, Elguero J (2000) Behaviour of ylides containing N, O and C atoms as hydrogen bond acceptors. J Am Chem Soc 122:11154–11161
42. Nouri A, Mirzaei M (2009) DFT calculations of B-11 and N-15 NMR parameters in BN nanocone. J Mol Struct: THEOCHEM 913:207–209